CrossMark

J. Fluid Mech. (2017), *vol.* 814, *pp.* 277–300. © Cambridge University Press 2017
doi:10.1017/jfm.2016.852

Colliding drops as coalescing and fragmenting liquid springs

C. Planchette[1,†], H. Hinterbichler[1], M. Liu[2], D. Bothe[2] and G. Brenn[1]

[1]Institute of Fluid Mechanics and Heat Transfer, Graz University of Technology, Inffeldgasse 25/F, 8010 Graz, Austria

[2]Center of Smart Interfaces, Darmstadt University of Technology, Alarich-Weiss-Straße 10, 64287 Darmstadt, Germany

(Received 4 May 2016; revised 12 December 2016; accepted 12 December 2016; first published online 3 February 2017)

A universal modelling approach of drop fragmentation after head-on drop collisions is presented. In this approach, the colliding drops are seen as liquid springs that coalesce, compress and relax, leading the merged drop to break up if it reaches a critical aspect ratio. Combining energetic balance of the compression and relaxation phases with a Rayleigh-like criterion, we deduce the fragmentation threshold velocity for the collision of two and three drops of the same liquid and of two drops of immiscible liquids. Predictions and experimental results obtained for these three kinds of collisions using various liquids and drop sizes are found to be in good agreement over a wide domain whose boundaries are discussed.

Key words: breakup/coalescence, capillary flows, drops

1. Introduction

Drop collisions have been of scientific interest since more than a century. Primary interest emerged from meteorology for the relevance of droplet coalescence for explaining rates of rainfall (Montgomery 1970). Detailed experimental studies revealed the importance of the drop kinetic and surface energies as well as the impact parameter for the outcomes from binary collisions (Brazier-Smith, Jennings & Latham 1972; Ashgriz & Poo 1990). The transition between coalescence and fragmentation for head-on binary drop collisions has been intensely studied due to its technical importance for numerous processes involving aerosols and sprays or aiming to produce droplets such as printing and atomization. Ashgriz & Poo (1990) focused on water drops and described the transition between coalescence and fragmentation with the help of a critical Weber number, derived from the assumption of a purely inviscid regime. Jiang, Umemura & Law (1992) introduced viscous losses in their study of alkane drop collisions with Ohnesorge numbers varying between 0.007 and 0.04. The authors divided the collision into two subsequent phases and found that the viscous losses of the first phase, until the merged drop reaches its maximal compression, are independent of the liquid viscosity, purely inertial and corresponding to a fixed fraction (approximately 50 %) of the initial kinetic energy.

† Email address for correspondence: carole.planchette@tugraz.at

https://doi.org/10.1017/jfm.2016.852 Published online by Cambridge University Press

They also proposed a model based on an energy balance that predicts the transition to occur for a critical Weber number that increases linearly with the ratio of viscosity and surface tension. Qian & Law (1997) refined this model dividing the collisions in three phases instead of two. The first phase and the associated losses are unchanged, but further developments are proposed for the losses in the subsequent phases. The result predicts a fragmentation transition for a critical Weber number that scales linearly with the drop Ohnesorge number. The theoretical work of Roisman (2009*a*), which focuses on the first phase of inertia-dominated drop collisions, predicts that the losses are inertial, in agreement with the experimental results of Jiang *et al.* (1992). The subsequent collision evolution is not addressed by Roisman (2009*a*) and thus no attempt to model the fragmentation threshold is made. The onset of fragmentation found and modelled by Qian & Law (1997) could be reproduced in the numerical work of Lycett-Brown *et al.* (2014). Yet, the experimental study of Willis & Orme (2003), involving Ohnesorge numbers larger than 0.3, showed that the losses in the first phase are not inertial but rather increase with increasing viscosity. No modelling is proposed in this study, but various numerical simulations seem to indicate a similar trend (Dai & Schmidt 2005; Nikolopoulos, Nikas & Bergeles 2009; Saroka, Ashgriz & Movassat 2012) which is expected to affect the fragmentation threshold predictions mentioned above. Indeed, Gotaas *et al.* (2007) experimentally observed that, for Ohnesorge numbers greater than 0.04, the transition between coalescence and fragmentation could not be described by the model of Qian & Law (1997) any more. No modelling was proposed to quantify this effect. In the present paper, we thus propose to carefully investigate both the losses at the end of first phase, when the drops have reached their maximal compression, and the fragmentation threshold including regimes with low Ohnesorge and high Reynolds numbers, for binary drop collisions using a single liquid. Our modelling approach being general, making use of the analogy between drops and liquid springs and of a Rayleigh-like criterion for fragmentation, extends beyond binary drop collisions with a single liquid and treats two other kinds of drop collisions: the collisions between two drops of immiscible liquids and the collisions between three drops of one single liquid. The motivation to include collisions between immiscible liquid drops and between three drops arises from the increasing interest in using drop collisions for various applications. Indeed, two colliding drops of different liquids constitute a microreactor which is of interest for example for combustion (Chen & Chen 2006). Such a process can also be used to produce microcapsules with a solid or liquid shell as proposed by Yeo *et al.* (2004) and Planchette, Lorenceau & Brenn (2012) and the combination of more than two drops (Hinterbichler, Planchette & Brenn 2015) opens the way for greater complexity of microreactors and microcapsules. Regardless of the number of drops or the nature of the liquids involved, the description of the boundaries between various regimes of collision outcomes is of critical importance, and among them the onset of fragmentation appears essential. Thus, in the present paper, scaling laws are derived, especially for the losses at the end of the compression and for the fragmentation threshold, that are systematically compared to the experimental data for each of the three studied kinds of collisions.

In the following section, we present the materials and methods used in the experiments. Section 3 consists of the modelling itself and is divided in subsections that successively focus on the compression phase, the fragmentation criterion, the relaxation phase and the onset of fragmentation itself. The paper ends with the summary and conclusions.

https://doi.org/10.1017/jfm.2016.852 Published online by Cambridge University Press

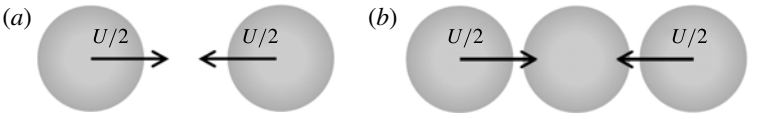


FIGURE 1. (*a*) Binary head-on collision. (*b*) Ternary symmetric head-on collision. The collisions are represented in the reference system moving with the drops centre of mass.

2. Materials and experimental methods

The present work focuses on head-on and symmetric collisions of two or three droplets of equal diameter D. The term head-on designates collisions involving drops whose centres of mass are aligned with the direction of their relative velocity. In the case of ternary collisions, symmetric indicates that the central drop moves with the centre of mass of the system and constitutes a centre of symmetry. The relative velocity U is defined between the outer drops, as represented in figure 1.

The experimental data of this study correspond to those of Planchette *et al.* (2012) and Hinterbichler *et al.* (2015), completed by new data obtained in the same manner which we briefly recall for completeness. Controlled drop collisions were produced by adjusting the relative position and orientation of two or three streams of regularly spaced monodisperse liquid droplets with diameters between 130 and 870 μm. Pictures of the drop collisions were recorded which allow for the determination of the drop diameters D and the relative velocity U by image analysis using the public domain software ImageJ (https://imagej.nih.gov/ij/). The procedure and experimental set-up are described in more detail elsewhere (Planchette *et al.* 2012; Hinterbichler *et al.* 2015). The liquids used in this study comprise aqueous glycerol solutions, silicon oils and perfluorodecalin, covering wide ranges of density $887 < \rho < 1935$ kg m^{-3}, dynamic viscosity $1.2 < \mu < 19.3$ mPa s and surface tension $17.8 < \sigma < 68.9$ mN m^{-1}.

Illustrative photographs of drop collisions below and above the fragmentation threshold are reproduced in figure 2 for ternary and binary cases involving one single or two immiscible liquids. The drops move from top to bottom.

3. Modelling of drop collisions

Drop collisions involve the conversion of energy from the kinetic and surface forms into surface and, *a priori*, kinetic energies. This conversion is subject to viscous losses and possibly leads to the fragmentation of the merged entity. Our modelling approach, schematically represented in figure 3, is based on the following aspects. First, the drops are seen as liquid springs (Richard, Clanet & Quéré 2002; Okumura *et al.* 2003; Biance *et al.* 2006) which undergo a strong distortion similar to an oscillation. As done by Jiang *et al.* (1992), we subdivide the deformation of the drops into two phases. The first phase extends from the instant of impact to the state of maximum extension of the disk-shaped entity. The second phase corresponds to the relaxation of the deformed entity into a transversely elongated, nearly cylindrical shape. By analogy with a spring system, we refer to the first phase as to a compression and to the second one as to a relaxation. Secondly, energy can be balanced for the compression, using an appropriate time scale and neglecting the internal kinetic energy at maximum deformation. From the description of the liquid complex at the end of the compression, we deduce its evolution during relaxation. Finally, fragmentation occurs if the cylinder formed during relaxation reaches a critical aspect ratio ζ_{crit} close

https://doi.org/10.1017/jfm.2016.852 Published online by Cambridge University Press

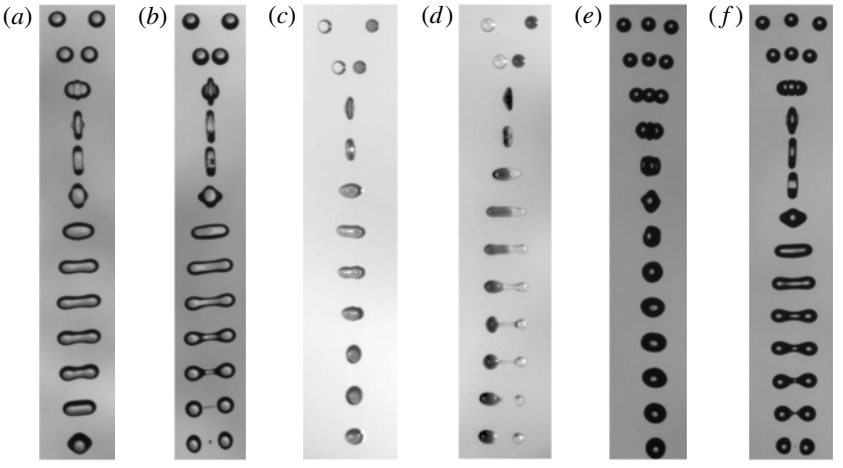


FIGURE 2. (*a*,*b*) Binary collisions of 50 % glycerol solution drops. (*a*) Coalescence, $U = 2.11$ m s^{-1}; (*b*) fragmentation, $U = 2.74$ m s^{-1}. (*c*,*d*) Binary collisions of drops of a 50 % glycerol solution (dark) and of silicon oil (transparent). (*c*) Full encapsulation (SO M20), $U = 3.88$ m s^{-1}; (*d*) fragmentation (SO M5), $U = 3.97$ m s^{-1}. (*e*,*f*) Ternary collisions of 50 % glycerol solution drops. (*e*) Coalescence, $U = 1.72$ m s^{-1}; (*f*) fragmentation, $U = 2.94$ m s^{-1}. All drops have diameters of 350 ± 15 μm. The time span between two successive pairs or triplets of drops is 160 ± 20 μs.

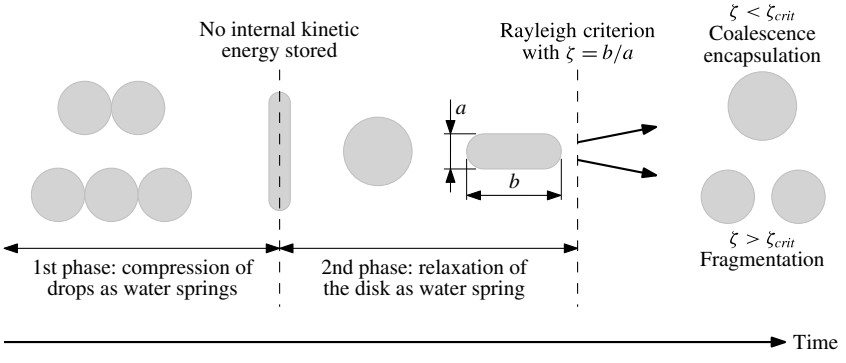


FIGURE 3. Illustration of the modelling approach considering drops as liquid springs that merge and distort analogously to an oscillation. The fragmentation of the merged entity occurs if its aspect ratio ζ exceeds a critical value.

to the one predicted as unstable by the Rayleigh criterion. These aspects are discussed below in the following sequence: the compression, the fragmentation criterion, the relaxation, and finally the resulting threshold.

3.1. *Compression*

3.1.1. *Time scale of compression*

Following the analogy between drops and springs, the time period needed for the liquid complex to reach its maximal diameter, t_{Dmax}, is expected to be a fraction of one drop oscillation period. According to Rayleigh's theory (Rayleigh 1879), the

https://doi.org/10.1017/jfm.2016.852 Published online by Cambridge University Press

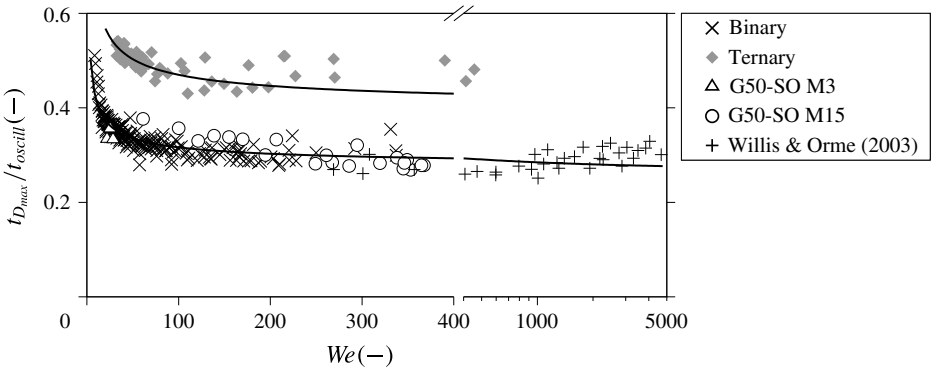


FIGURE 4. t_{Dmax}/t_{oscill} as a function of We for binary collisions with one liquid: our data (×), the data of Willis & Orme (2003) (+), for binary collisions with immiscible liquids (glycerol at 50 % and silicon oil M3 (△) or silicon oil M15 (○), and for ternary collisions (◆). Solid lines correspond to the semi empirical time scale given by (3.1).

oscillation period of a drop of mass $\pi\rho D^3/6$ and surface tension σ is proportional to $t_{oscill} = \sqrt{\rho D^3/\sigma}$ where σ is equivalent to a spring constant. This scaling differs from $t_{Dmax} \approx D/U$ which has been commonly used in most of the studies (Jiang *et al.* 1992; Qian & Law 1997). Using the collision photographs, we have recorded the temporal evolution of the disk diameter and deduced t_{Dmax} as described in Roisman *et al.* (2011). The measurements were performed for the three kinds of collisions using a wide range of liquid properties ($1.2 < \mu < 19.3$ mPa s and $17.8 < \sigma < 68.9$ mN m^{-1}), of drop sizes ($130 < D < 870$ μm) and considering velocities below and above the threshold of fragmentation ($1 < U < 7$ m s^{-1}). The data of Willis & Orme (2003) provide t_{Dmax} for other conditions ($\mu = 10$ and 30 mPa s, $\sigma = 20$ mN m^{-1}, $400 < D < 700$ μm, $3 < U < 14$ m s^{-1}), sometimes far above the threshold of fragmentation. We have plotted in figure 4 the ratio of the measured t_{Dmax} to t_{oscill} as a function of the Weber number, defined by $We = \rho D U^2/\sigma$ for both binary and ternary collisions with one single liquid. For collisions with immiscible liquids, t_{oscill} and We are defined using the properties of the aqueous drop.

We observe two main regimes corresponding to low and large We, with a transition around $We = 50$. For large We ($50 < We$), the proportionality between t_{Dmax} and t_{oscill} is excellent. We selected the data corresponding to $50 < We$ and plotted t_{Dmax} as a function of t_{oscill} in figure 5(*a*). For binary collisions, the slope between t_{Dmax} and t_{oscill} is found to be 0.32. The data of Willis & Orme (2003), which correspond to larger Oh, show small deviations. The deviations, decreasing with increasing U may be attributed to a change toward a viscous-dominated regime. Using immiscible liquids (silicon oils M3 and M15 with a 50 % glycerol solution), t_{Dmax} of the aqueous drop (glycerol at 50 %) is recovered. The proportionality between t_{Dmax} and t_{oscill} is also observed for ternary drop collisions. In this case, the slope is found to be 0.49, indicating that for ternary drop collisions the disk takes 1.5 times longer to reach its maximal extension than for binary collisions. This ratio can be explained considering the association of identical springs in a series. Each of these identical springs has a mass $\pi\rho D^3/6$ and a spring constant σ. In the case of binary collisions, two such identical springs are associated in a series, forming an equivalent spring whose mass is $2\pi\rho D^3/6$ and spring constant is $\sigma/2$ (Symon 1971). t_{Dmax} is thus expected to be proportional to $2\sqrt{\rho D^3/\sigma}$. Similarly, for ternary collisions, the equivalent spring corresponding to the

https://doi.org/10.1017/jfm.2016.852 Published online by Cambridge University Press

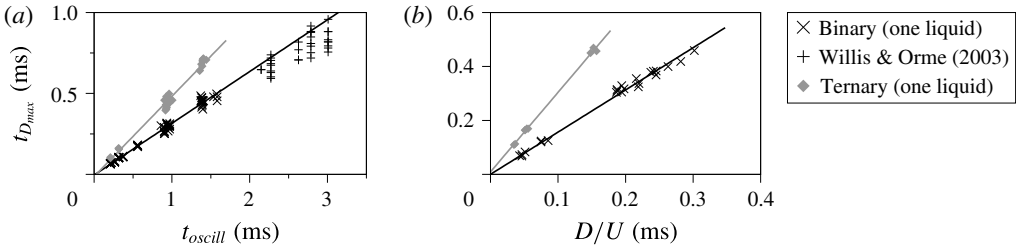


FIGURE 5. t_{Dmax} as a function of (*a*) t_{oscill} for $We > 50$ and (*b*) D/U for $We < 20$ and $We < 40$ for binary and ternary collisions, respectively. Binary collisions, our data (×), data from Willis & Orme (2003) (+) and ternary collisions (◆).

association of three identical springs in a series is expected to give t_{Dmax} proportional to $3\sqrt{\rho D^3/\sigma}$. The theoretical ratio between the time period obtained with three drops and two drops is thus 3/2, as found experimentally.

For low We ($We < 50$), the dynamic pressure cannot overcome the Laplace pressure. The drops being too 'hard' to be 'compressed', they coalesce with their centre of mass moving at approximately $U/2$. t_{Dmax} is of the order of D/U as shown in the figure 5(*b*) where t_{Dmax} is plotted as a function of D/U for $We < 20$ and $We < 40$ for binary and ternary collisions, respectively. The ratio of the slopes, 1.9, is close to the theoretically expected value of 2.

From this analysis we deduce that, for binary and ternary collisions, t_{Dmax} scales with t_{oscill} for high We and with D/U for low We. At intermediate We, both time scales are of the same order of magnitude. As suggested by Bazilevskii *et al.* (1981), summing up the two time scales provides an overall good approximation of t_{Dmax} which thus writes

$$t_{Dmax} = \alpha(t_{oscill} + \beta D/U). \tag{3.1}$$

Linear least squares fitting provides values of α equal to 0.27 and 0.39 and β equal to 1.72 and 2.05, as plotted in figure 4, for single liquid binary and ternary collisions, respectively. For binary collisions with immiscible liquids, the instant of maximal extension is similar to the one expected using two drops of the aqueous solution.

3.1.2. *Energy balance*

The general formulation of the energy balance for the compression phase reads:

$$E_{K,ini} + E_{\sigma,ini} = E_{K,disk} + E_{\sigma,disk} + E_{\mu,comp}, \tag{3.2}$$

where $E_{K,ini}$ is the initial kinetic energy, $E_{\sigma,ini}$ the initial surface energy, $E_{K,disk}$ the kinetic energy stored within the disk at its maximal extension, $E_{\sigma,disk}$ the surface energy of the disk and $E_{\mu,comp}$ the viscous losses experienced during compression.

For the three kinds of collisions considered in this work, the initial energies are given by the equations listed in table 1. Similarly to the Weber number, we define for binary and ternary collisions with one liquid, the Reynolds and Ohnesorge numbers as $Re = \rho DU/\mu$ and $Oh = \mu/\sqrt{\rho D\sigma}$. For binary collisions with immiscible liquids, these numbers will be defined in the discussion.

3.1.3. *Neglecting* $E_{K,disk}$

In most of the modelling approaches as from Jiang *et al.* (1992), Qian & Law (1997) and Planchette *et al.* (2012), it is common to assume that $E_{K,disk}$ is negligible. To our knowledge, no experimental observations have been published to confirm

https://doi.org/10.1017/jfm.2016.852 Published online by Cambridge University Press

Type of collision	$E_{K,ini}$	$E_{\sigma,ini}$
Binary (one liquid)	$\pi\rho D^3U^2/24$	$2\pi D^2\sigma$
Ternary (one liquid)	$\pi\rho D^3U^2/24$	$3\pi D^2\sigma$
Binary – immiscible liquids	$\pi(\rho_o+\rho_w)D^3U^2/48$	$\pi D^2(\sigma_o+\sigma_w)$

TABLE 1. Initial energies for the three types of drop collisions considered in this work. For immiscible liquids, σ_o and σ_w correspond to the surface tensions of the oil and of the aqueous solution, respectively.

this hypothesis. Numerical studies, however, seem to support this assumption, as for example Nobari, Jan & Tryggvason (1996), Dai & Schmidt (2005) and Nikolopoulos *et al.* (2009).

In the present work, further evaluation of $E_{K,disk}$ has been preformed using numerical simulations. For simplicity and since the numerical simulations of binary collisions have already been successfully implemented and validated (Focke & Bothe 2011, 2012; Focke *et al.* 2013; Liu & Bothe 2016), we focus here on this type of collision. The numerical simulations were performed with the in-house code Free Surface 3D (FS3D) that is based on the Volume-of-Fluid (VOF) method (Hirt & Nichols 1981). In the simulations, the further improved version of the lamella stabilization algorithm from Liu & Bothe (2016) is employed in order to prevent the unphysical lamella rupture at higher Weber numbers as described in Focke & Bothe (2011), Focke & Bothe (2012) and Liu & Bothe (2016). The surface tension force is incorporated by means of the continuum surface stress (CSS) model (Lafaurie *et al.* 1994). All simulations are conducted using a computational domain of 500 μm $\times$ 500 μm $\times$ 1000 μm and 128 $\times$ 128 $\times$ 256 grid cells with three symmetry planes, resulting in a resolution of at least 87 cells per drop diameter.

Four cases are selected that correspond to experimentally investigated conditions. The drop diameter is fixed to 340 μm, glycerol solution at 50 % and silicon oil M5 are considered, and for each of these two liquids two relative drop velocities are considered: one leading to coalescence and one resulting in fragmentation. Expressed in terms of Oh and We, the four cases correspond to $Oh = 0.03$ (glycerol 50 %) with $We = 25$ and 56 and $Oh = 0.06$ (silicon oil) with $We = 35$ and 69. The shape of the drops obtained from the simulation are very similar to the ones observed in the experiments, as shown in figure 6 for the case $Oh = 0.03$.

The temporal evolution of the different energetic contributions, as found in the numerical simulations, are presented in figure 7. At the instant of maximal disk extension – marked by black vertical lines – the internal kinetic energy represents less than 2 % of the total energy, and so for Oh equal to 0.03 and 0.06, below and above the critical velocity of fragmentation. Together with the results of Nobari *et al.* (1996), Dai & Schmidt (2005) and Nikolopoulos *et al.* (2009), these findings validate the assumption that the internal kinetic energy at the end of the compression is negligible for a wide range of Oh (0.02–0.38). Generalizing this result to other kinds of drop collisions, (3.2) can be approximated by

$$E_{K,ini} + E_{\sigma,ini} = E_{\sigma,disk} + E_{\mu,comp}. \tag{3.3}$$

3.1.4. *Estimating $E_{\mu,comp}$ via scaling argument*

In this section we propose to estimate $E_{\mu,comp}$ based on scaling arguments. The results, established for binary collisions, are later compared to numerical and experimental data.

https://doi.org/10.1017/jfm.2016.852 Published online by Cambridge University Press

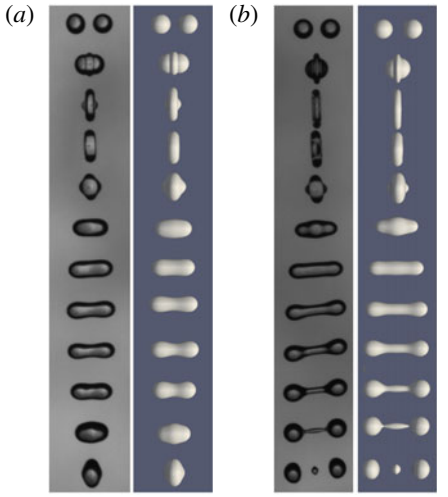


FIGURE 6. (Colour online) Temporal evolution of the drop shapes after collision as observed in experiments and obtained by numerical simulations. $Oh = 0.03$. (*a*) $We = 25$. (*b*) $We = 56$.

Despite the similarity between binary drop collisions and impact of drops on solid walls, scaling relations cannot be interchanged due to the development of a viscous boundary layer at the vicinity of the wall (Roisman 2009*b*). It is therefore crucial to figure out where the viscous losses take place for binary drop collisions. Nikolopoulos *et al.* (2009) numerically calculated the viscous losses taking place both in the liquid and gaseous phases and showed that losses in the surrounding gaseous phase are a small fraction of the total losses. Thus, thereafter, only the liquid phase is considered. The numerical simulations by Nobari *et al.* (1996) indicate that, for bouncing drops, i.e. small *We*, the highest dissipation per unit volume is found at the outer edges of the drops and not in a thin layer near the stagnation point as proposed by Jiang *et al.* (1992). Roisman (2004), Roisman *et al.* (2011) who focused on the inertia-dominated regime (high *We* and *Re*), localized the losses in the lamella just upstream from the rim and, to a smaller extend, in the rim itself. Accounting for these findings, we propose different possible locations of the losses. We then estimate the losses and discuss the regime where they may dominate.

(i) Losses in the lamella – just upstream from the rim: $E_{\mu,comp,1}$.

For the inertia-dominated regime, the liquid flows from the centre of the disk towards its outer edge, where it is slowed down by surface tension forcing the liquid to accumulate in a rim. The biggest velocity gradients are thus found in the lamella just upstream from the rim, see figure 8. The difference of velocities between the flow in the rim and in the lamella can be approximated by U, while the length scale of deceleration is the one of the viscous boundary layer developing just in front of the rim. As a consequence:

$$E_{\mu,comp,1} \approx \mu \left(\frac{U}{l_\mu}\right)^2 \Omega_1 T_1, \tag{3.4}$$

with $l_\mu \approx \mu/\rho U$. The volume Ω_1 on which this dissipation occurs is the volume of a crown of width l_μ and thickness h, the thickness of the lamella close to the rim. The

https://doi.org/10.1017/jfm.2016.852 Published online by Cambridge University Press

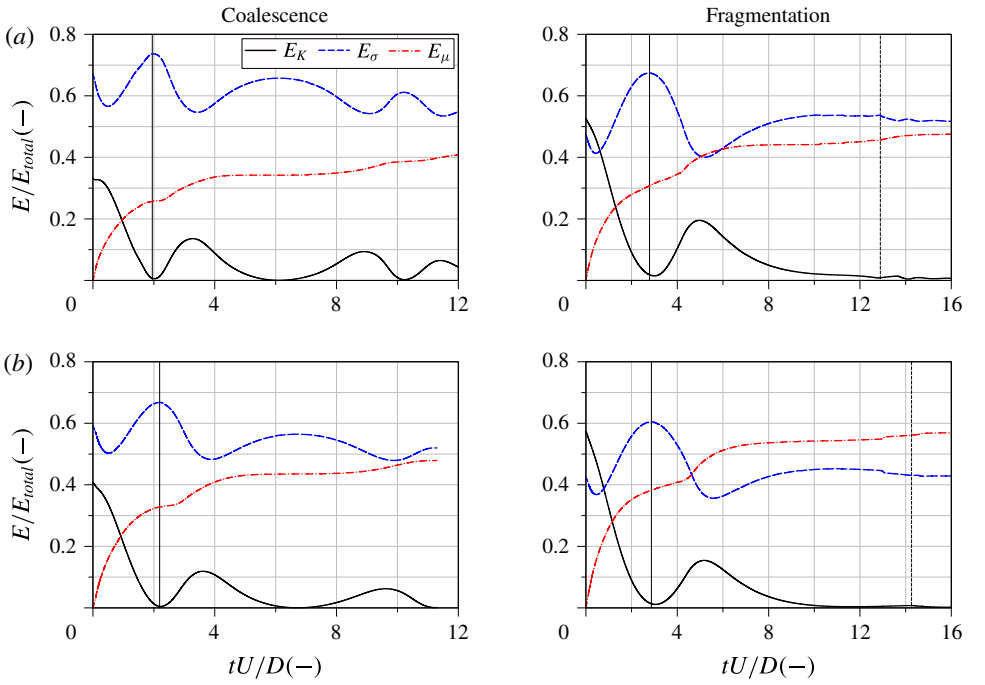


FIGURE 7. (Colour online) Temporal evolution of the surface and kinetic energies, and of the accumulated viscous losses during the compression phase of binary drop collisions (E_{total} is the sum of E_K, E_σ and E_μ). From left to right: (*a*) $Oh = 0.03$, $We = 25$ and $We = 56$; (*b*) $Oh = 0.06$, $We = 35$ and $We = 69$. The black vertical lines (solid) mark the maximal extension of the disk. The kinetic energy in that state is below 2 % of the initial energy for all cases. The dashed vertical lines mark the break up of the liquid cylinder formed during relaxation.

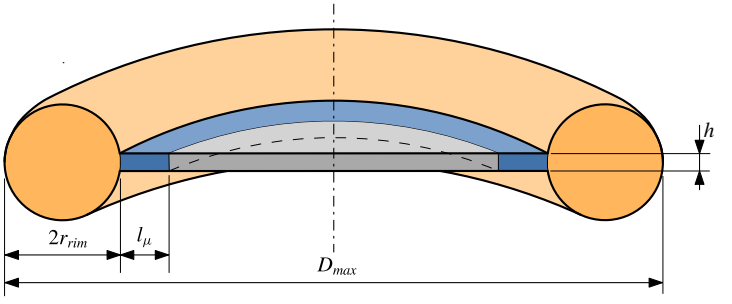


FIGURE 8. (Colour online) Schematic representation of liquid complex during compression (cut in the centre) showing the two main locations of viscous losses. The blue crown corresponds to the volume in the lamella while the orange torus is the rim volume.

diameter of the crown can be approximated by D_{max}, the maximum diameter of the disk, which scales at first order like $D\sqrt{We}$ (Jiang *et al.* 1992; Willis & Orme 2000, experimental results of § 3.1.6). As in Roisman (2004) and Roisman *et al.* (2011), we use the result of Taylor (1959) to estimate $h \approx \sigma/2\rho U^2$.

https://doi.org/10.1017/jfm.2016.852 Published online by Cambridge University Press

The time period T_1 on which these losses develop could at first be estimated by t_{Dmax}. In the first instants of the collision, however, the lamella is not yet formed, and approximating T_1 by t_{oscill} seems more appropriate here.

We obtain

$$E_{\mu,comp,1} \propto \rho D^3 U^2. \tag{3.5}$$

Note that taking $T_1 \approx t_{Dmax}$ would influence the proposed scaling only for small *We* which does not correspond to the inertia-dominated regime.

(ii) Losses in the rim: $E_{\mu,comp,2}$.

In the work of Roisman *et al.* (2011) focusing on the inertia-dominated regime, losses in the rim are added to the dominating ones taking place in the lamella. The velocity in the rim is approximated by the interface velocity, itself derived from volume conservation between the lamella and the rim. The length scale of the velocity gradient is estimated by l_μ. With these assumptions, the losses in the rim scale as those of the lamella but are found to be much smaller.

We propose here an alternative scaling that accounts for smaller *Re*, i.e. going beyond the limit of inertia-dominated regime. In the rim, capillary effects dominate over inertia and the liquid velocity can be estimated by $V_{rim} \approx \sqrt{\sigma/\rho r_{rim}}$ where r_{rim} designates the rim radius. This velocity is expected to be much smaller than the one in the lamella, and for high viscosity, the viscous boundary layer in the rim becomes probably as large as the radius of the rim itself. Thus, the losses in the rim are:

$$E_{\mu,comp,2} \approx \mu \left(\frac{V_{rim}}{r_{rim}}\right)^2 \Omega_2 T_2. \tag{3.6}$$

Noting that the lamella is very thin and does not represent a significant volume of liquid, volume conservation allows writing $r_{rim} \approx DWe^{-1/4}$. The volume Ω_2 on which these losses occur corresponds to the rim volume, i.e. to $r_{rim}^2 D_{max} \propto D^3$, in orange in figure 8. The time period T_2 can be taken as t_{Dmax}, since the rim starts forming immediately after impact. In this case, we obtain:

$$E_{\mu,comp,2} \propto \rho D^3 U^2 \frac{We^{1/4} + \beta We^{-1/4}}{Re}. \tag{3.7}$$

This expression is valid if the viscous boundary layer thickness becomes effectively comparable to the rim radius, i.e. in the limit of small *Re*. Note that approximating T_2 by t_{oscill} would result in $E_{\mu,comp,2} \propto \rho D^3 U^2 We^{1/4} Re^{-1}$. Differences would be mainly found for low *We*, where the drops hardly deform into a lamella.

(iii) Low *Oh*: $E_{\mu,comp,3}$.

We observe for collisions at low *Oh* that the lamella is less pronounced and its diameter remains small in comparison to D_{max}, while it is surrounded by a large rim. We attribute this difference to the strong capillarity (small *We*), which limits the extension of the disk and possibly to the low viscosity (high *Re*) which slows down the flow development. It is worth noting that $Oh = t_{oscill}/t_\mu$ and consequently $Oh \approx t_{Dmax}/t_\mu$, with the viscous time scale $t_\mu = \rho D^2/\mu$. In the case of low *Oh*, and hence low t_{Dmax}/t_μ, the viscous boundary layer may not have enough time to fully develop before the disk recoils. Let us thus consider a viscous layer of thickness $l_\mu^* = \sqrt{(\mu/\rho)t_{Dmax}}$ ($\ll l_\mu$). The losses can be obtained by integrating $\mu U^2/{l_\mu^*}^2$ over t_{Dmax} in a volume proportional to $D^2 l_\mu^*$. The losses are expected to scale as $\rho D^3 U^2 \sqrt{t_{Dmax}/t_\mu}$.

https://doi.org/10.1017/jfm.2016.852 Published online by Cambridge University Press

Approximating t_{Dmax} by t_{oscill} is equivalent to neglecting β by comparison to $\sqrt{We}$ and seems practically acceptable for all fragmentation conditions ($\beta < \sqrt{We}$ for $We > 3$). Thus, we obtain:

$$E_{\mu,comp,3} \propto \rho D^3 U^2 \sqrt{Oh}. \tag{3.8}$$

This analysis offers three kinds of losses. For small Oh, the lamella does not totally develop and (3.8) is expected to apply. When the lamella forms, purely inertial losses are expected that scale as predicted by (3.5). In the limit of low Re, additional losses in the rim must be added which follow the scaling of (3.7).

3.1.5. *Surface at maximal deformation*

To compare the predictions of (3.5), (3.7) and (3.8) with the experimental results, we first evaluate $E_{\sigma,disk}$ from collision photographs. $E_{\mu,comp}$ is obtained in a second step via (3.3). Yet, the exact shape of the liquid complex at maximal extension is difficult to describe, and the radius of the rim is difficult to measure. In the case of binary collisions, Willis & Orme (2003) showed that this surface can be well approximated by the one of a pancake of diameter D_{max} and thickness $e \approx 4/3\, D^3 D_{max}^{-2}$ (volume conservation). The difference from the surface of a torus of the same maximal diameter was found to be of the order of typical experimental uncertainty. Thus, we estimate the surface energy of the liquid complex at its maximal extension by:

$$E_{\sigma,disk} = \frac{\pi}{2}\sigma {D_{max}}^2 \left(1 + \frac{8}{3}\left(\frac{D}{D_{max}}\right)^3\right). \tag{3.9}$$

This estimation is in good agreement with the numerical simulations. For $Oh = 0.03$ and $D_{max}/D = 1.80$ (or $D_{max}/D = 2.10$), we obtain $E_{\sigma,disk}/E_{\sigma,ini}$ equal to 1.18 (or 1.42) using (3.9), and to 1.11 (or 1.44) from the simulations. For $Oh = 0.06$, with $D_{max}/D = 1.85$ (or $D_{max}/D = 2.13$), $E_{\sigma,disk}/E_{\sigma,ini}$ equals 1.20 (or 1.43) with (3.9), and 1.13 (or 1.42) from the simulations. The differences decrease with increasing D_{max}/D and remain below 7 % for $D_{max}/D > 1.8$ validating the use of (3.9).

For binary drop collisions with immiscible liquids, we use by analogy

$$E_{\sigma,disk} = \frac{\pi}{2}{D_{max}}^2 \left((\sigma_o + \sigma_{ow}) + \frac{8}{3}\left(\frac{D}{D_{max}}\right)^3 \left(\sigma_o + \frac{\sigma_{ow}}{2}\right)\right) \tag{3.10}$$

and in the ternary case

$$E_{\sigma,disk} = \frac{\pi}{2}\sigma {D_{max}}^2 \left(1 + 4\left(\frac{D}{D_{max}}\right)^3\right). \tag{3.11}$$

3.1.6. *Experimental estimation of* $E_{\mu,comp}$

For each liquid and droplet size we vary U, measure D_{max} on the photographs, obtain the experimental $E_{\sigma,disk}$ and further compute $E_{\mu,comp}$ which we plot as a function of $E_{K,ini}$. This approach is similar to the one followed by Jiang *et al.* (1992) and Willis & Orme (2003), where the evolution of $\hat{S} = E_{\sigma,disk}/E_{\sigma,ini}$ with $We^* = E_{K,ini}/E_{\sigma,ini}$ was studied. Indeed, noting $E_{\mu,comp} = f(E_{K,ini})$ gives $\hat{S} = 1 + We^* - f(We^*)$. Since it has

https://doi.org/10.1017/jfm.2016.852 Published online by Cambridge University Press

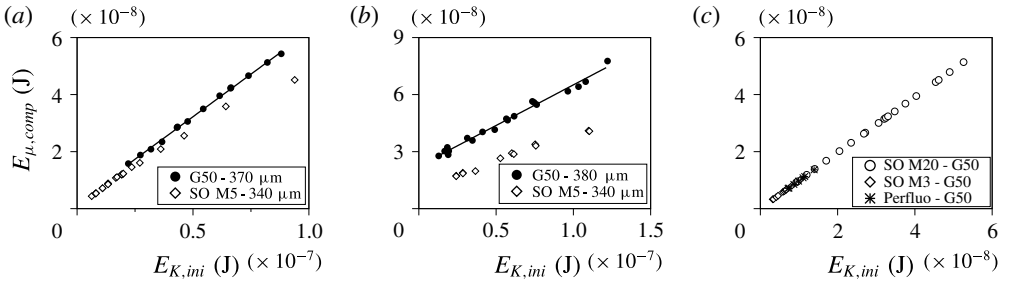


FIGURE 9. Examples of $E_{\mu,comp}$ as a function of $E_{K,ini}$. (*a*) Binary collisions with one liquid, (*b*) ternary collisions, (*c*) binary collisions with immiscible liquids ($D = 200$ µm). For wide ranges of U, deviations to the expected linear relation are observed (*a*) and (*b*) with SO M5.

been reported that $\hat{S}$ linearly increases with We^* (Jiang *et al.* 1992; Willis & Orme 2003), $E_{\mu,comp}$ is expected to linearly increase with $E_{K,ini}$. Typical results are shown in figure 9 for each kind of collision.

As expected, $E_{\mu,comp}$ increases nearly linearly with $E_{K,ini}$, which implies that, at first order, D_{max} scales like $D\sqrt{We}$. For wide ranges of U, however, we observe some deviations. To our knowledge, the deviation from linearity has not been discussed in the literature so far but was already visible on the measurements of Willis & Orme (2003). To overcome this difficulty we restrict ourselves to velocity ranges for which the deviations from the linear evolution are not significant. As a result, for some cases, we obtain two different slopes, one for rather low velocities and the other one for large velocities. The local slope of $E_{\mu,comp}$ as a function of $E_{K,ini}$ is thus systematically recorded. We denote this local slope as a and calculate Re and We for the median value of U.

This procedure is followed for binary collisions with $0.007 < Oh < 0.12$, including aqueous solutions of glycerol and silicon oils, and drop diameters between 130 and 380 µm. The values corresponding to $0.1 < Oh < 0.33$ deduced from the data of Willis & Orme (2003) are also considered. For ternary collisions, the studied conditions correspond to $0.02 < Oh < 0.12$ with $130 < D < 380$ µm. Even though rather moderate D_{max}/D are found for low Oh, most of the linear fits are made for $D_{max}/D > 1.8$, excluding very large errors in estimating $E_{\sigma,disk}$. The results are shown in figure 10. In the upper graph, we have chosen to plot a as a function of $\alpha(We^{1/4} + \beta We^{-1/4})/Re$; a as a function of Oh, We and Re are successively plotted in the lower graphs. For binary collisions with immiscible liquids, we use We defined on the encapsulated drop only, since it fixes t_{Dmax}. At this stage of the collision, the viscous losses are assumed to happen in both phases, thus an average Reynolds number defined as $\tilde{Re} = (\rho_o + \rho_w)DU/(\mu_o + \mu_w)$ is used.

For every kind of collision, we observe a plateau on which a is constant. For binary collisions with one liquid, this plateau is preceded and followed by different regimes. At low $\alpha(We^{1/4} + \beta We^{-1/4})/Re$, a fast increase of a is observed, while for large $\alpha(We^{1/4} + \beta We^{-1/4})/Re$ a rather moderate increase is visible. The value of a on the plateau indicates that 65 % of the initial kinetic energy has been lost at this stage of the process. For ternary collisions, only two of the three regimes are seen. The plateau at moderate $\alpha(We^{1/4} + \beta We^{-1/4})/Re$, which corresponds to a loss of 44 % of the initial kinetic energy, and the regime for larger $\alpha(We^{1/4} + \beta We^{-1/4})/Re$, where a slightly increases. The absence of experimental points for very low $\alpha(We^{1/4} + \beta We^{-1/4})/Re$

https://doi.org/10.1017/jfm.2016.852 Published online by Cambridge University Press

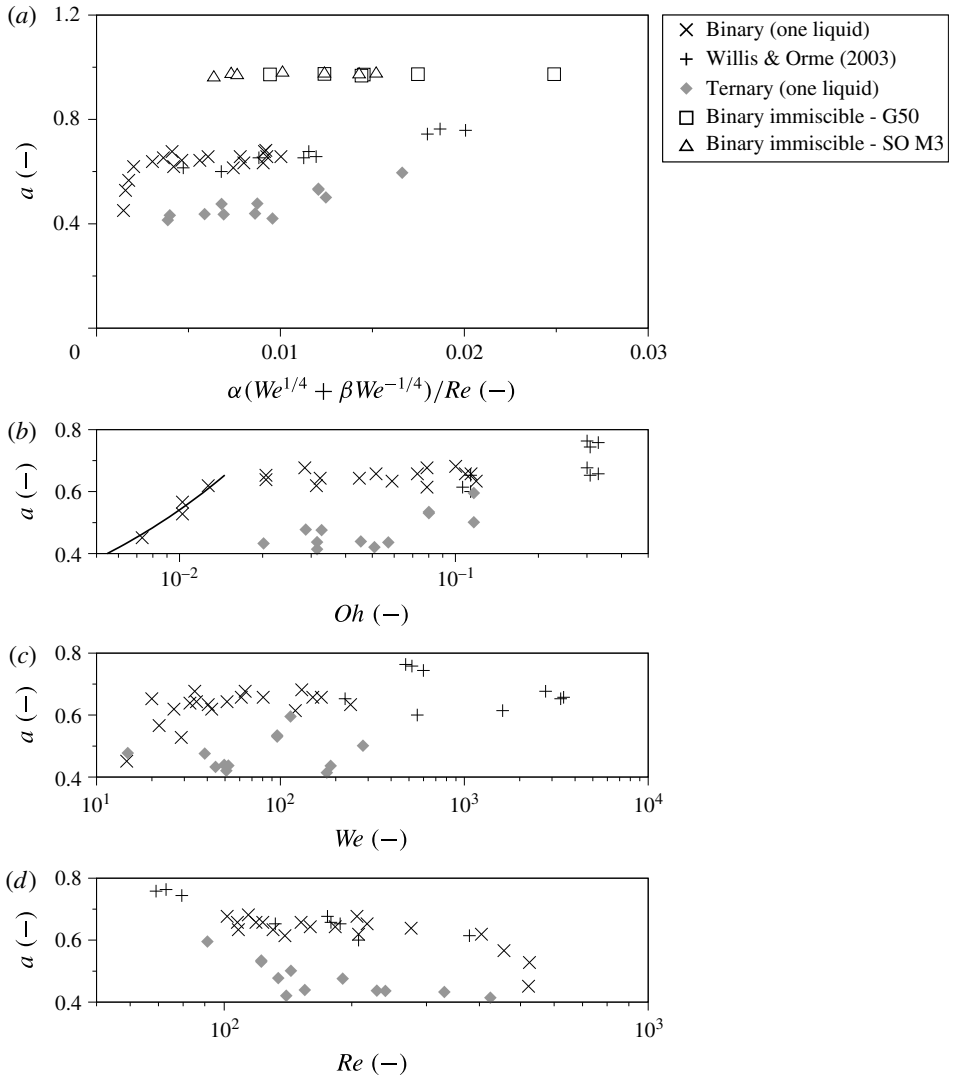


FIGURE 10. (*a*) a (slope of $E_{\mu,comp}$ as a function of $E_{K,ini}$) as a function $\alpha(We^{1/4} + \beta We^{-1/4})/Re$. For collisions with one liquid, binary ($\times$ and $+$) $\alpha = 0.27$, $\beta = 1.72$ and ternary collisions ($\blacklozenge$) $\alpha = 0.39$, $\beta = 2.05$. For binary collisions of immiscible liquid drops ($\triangle$ and $\square$) $\alpha = 0.27$, $\beta = 1.72$, We is defined with the encapsulated liquid properties and Re is taken as $(\rho_o + \rho_w)DU/(\mu_o + \mu_w)$. (*b–d*) a, (same points, one liquid) as a function of Oh, We and Re from top to bottom. Black line, (3.8).

can explain that the first regime of fast increase is not observed. Finally, for binary collisions of immiscible liquid drops, only the plateau is visible. Considering the wide range of parameters probed, the sensitivity of viscous dissipation to We and Re appears to be weak. The value of a is found to be 0.97, close to 0.96 as reported in Planchette *et al.* (2012), where the surface of the liquid complex at maximal extension was approximated by disks only. The dissipated energy during compression is thus much higher for immiscible liquid drops than for collisions with one single liquid.

https://doi.org/10.1017/jfm.2016.852 Published online by Cambridge University Press

3.1.7. *Discussion*

For binary collisions with one liquid, the results of figure 10 are in agreement with the findings of the literature. Indeed, the experimental results of Jiang *et al.* (1992), as well as the numerical results of Nobari *et al.* (1996), indicate that the amount of kinetic energy lost at the end of the compression phase is independent of μ, and therefore of Re. This corresponds to what we observe on the plateau of a for every kind of collision. Yet, it has also been observed (Willis & Orme 2003) and numerically calculated (Dai & Schmidt 2005; Nikolopoulos *et al.* 2009) that, for a certain range of Re, this loss of energy increases with decreasing Re, in agreement with our measurements for large $\alpha(We^{1/4} + \beta We^{-1/4})/Re$. Finally, the first regime observed for the binary collisions corresponds to points for which $Oh \approx 0.01$. The limited data published for this range of Oh do not allow for direct comparison.

The modelling approach of § 3.1.4 allows a qualitative interpretation of these results. Indeed, the data found on the plateau correspond to rather moderate or large Re and Oh ($100 < Re < 400$ and $130 < Re < 350$; $0.02 < Oh < 0.2$ and $0.02 < Oh < 0.08$ for binary and ternary collisions, respectively). In this regime, the viscous losses are mainly found in the lamella, just upstream from the rim, and are purely inertial (3.5), in agreement with Roisman *et al.* (2011). The losses are equal to approximately $a_{plat,2D} = 65\,\%$ and $a_{plat,3D} = 44\,\%$ of the initial kinetic energy for the binary and ternary collisions, respectively. Adapting the framework of non-dissipative water springs (see § 3.1.1) to linearly dissipative springs (spring constant σ, coefficient of linear dissipation μ) may help understanding the ratio of 1.48 between these values. Indeed, by associating 2 or 3 of such springs in a series, an equivalent spring of constant $\sigma/2$ or $\sigma/3$ is obtained, and similarly the coefficient of linear dissipation is changed to $\mu/2$ or $\mu/3$, respectively. For a given $E_{K,ini}$, the ratio of the losses (binary/ternary) is thus expected to approach the value of $3/2$. By reducing Re, the viscous boundary layer thickness may become comparable to the rim radius itself. Additional losses must be considered that mark the transition to the regime of large $\alpha(We^{1/4} + \beta We^{-1/4})/Re$. These losses take place in the rim and can be approached by (3.7). As predicted, the overall losses are greater than those of the lamella alone. The linear increase with $\alpha(We^{1/4} + \beta We^{-1/4})/Re$ is compatible with our data but should be further tested using a larger data set. Finally, the last regime observed for low $\alpha(We^{1/4} + \beta We^{-1/4})/Re$ may be equally well distinguished from the plateau considering low Oh. Equation (3.8) which describes losses for collisions where $t_{Dmax} \ll t_\mu$ is plotted in figure 10 as a black line. Beside the limited number of points, the agreement with the data is very good, supporting our interpretation.

To complete this analysis, we compare in figure 11 the experimental data for binary collisions to the numerical results of Dai & Schmidt (2005), Nikolopoulos *et al.* (2009) and Saroka *et al.* (2012). Nikolopoulos *et al.* (2009) varied Re, keeping We constant. Dai & Schmidt (2005) varied both Re and We and Saroka *et al.* (2012) considered three liquids with one drop size and varying velocities. Plotting the results of Dai & Schmidt (2005) as a function of $\alpha(We^{1/4} + \beta We^{-1/4})/Re$ brings the points along a single line, indicating the relevance of this parameter. For all mentioned studies, the plateau experimentally observed in our data and in Jiang *et al.* (1992) is not reproduced, and the curves are shifted towards small values of $\alpha(We^{1/4} + \beta We^{-1/4})/Re$. The missing plateau may indicate the difficulty for numerical simulations to model the losses within the lamella. The difficulties may arise from the small dimensions and large gradients, from numerical viscosity or from modelling the rupture of the gas layer. Indeed, in Nobari *et al.* (1996) it was shown that, by setting different instants of rupture, the velocity fields were modified. Thus, the shift

https://doi.org/10.1017/jfm.2016.852 Published online by Cambridge University Press

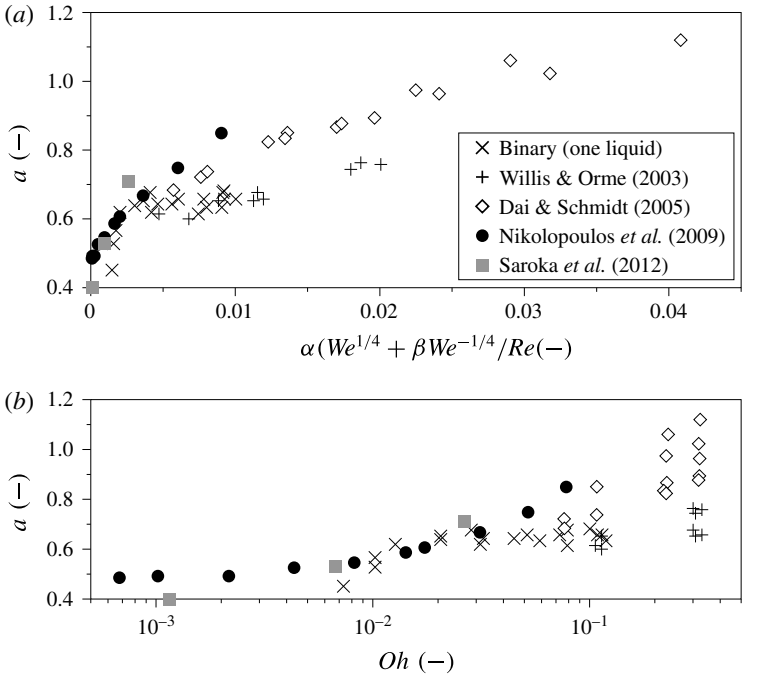


FIGURE 11. The slope a as a function of $\alpha(We^{1/4} + \beta We^{-1/4})/Re$, (*a*) and Oh, (*b*) for binary collisions. ($\times$ and $+$) Experimental results, (●, ◇ and ■) numerical results from Dai & Schmidt (2005), Nikolopoulos *et al.* (2009) and Saroka *et al.* (2012), respectively.

between experimental data and the results of Dai & Schmidt (2005) may originate from the initial velocity field set, which assumes the two drops to merge immediately after contact, while they are still spherical.

Finally, using immiscible liquid drops, only the plateau is visible (see figure 10). Given the wide range of parameters probed, the viscous dissipation appears weakly sensitive to We and Re. The value of a is found to be close to 0.97, much greater than for the two other studied configurations. Qualitatively, the presence of two immiscible liquids probably reduces the length scale of velocity variations, leading to higher gradients. The continuity of the shear stress at the interface, as well as the dynamic wetting of the aqueous phase by the oil, may also significantly modify the velocity field.

3.2. *Fragmentation criterion*

The usage of the Rayleigh criterion, normally applied to a static infinite liquid cylinder, was first proposed by Ashgriz & Poo (1990) for binary collisions of water drops and discussed by Planchette *et al.* (2012) for the case of two immiscible liquid drops. We presently extend it to binary and ternary collisions with one liquid. The maximal aspect ratio of the cylinder ζ is measured on photographs obtained around the fragmentation threshold – typically for velocities just below and above the transition, providing the lower and upper bounds of the critical value ζ_{crit}. A wide range of drop sizes ($130 < D < 550$ μm) and liquid properties ($1 < \mu < 20$ mPa s; $19 < \sigma < 70$ mN m^{-1}) were probed, corresponding to $0.007 < Oh < 0.18$. For immiscible liquids, Oh is here taken as the average of the two Oh obtained for the oil and the aqueous solution drops. The measurements are reproduced as a function of Oh for the three kinds of drop collisions in figure 12.

https://doi.org/10.1017/jfm.2016.852 Published online by Cambridge University Press

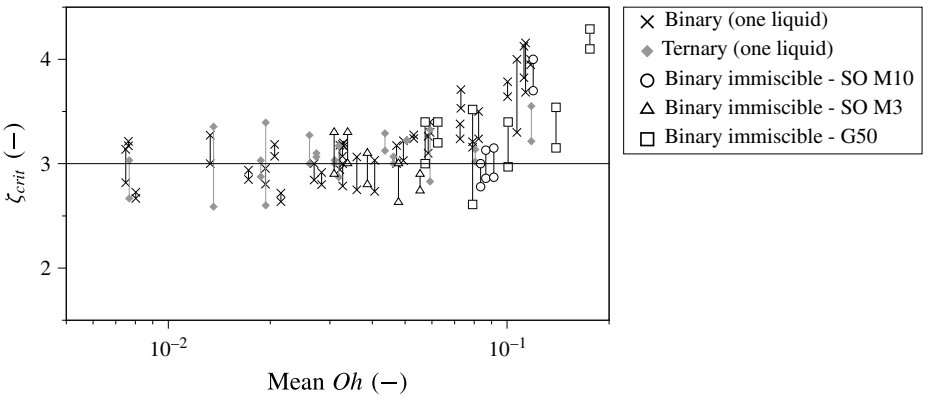


FIGURE 12. Critical aspect ratio of the cylinder ζ_{crit} as a function of Oh for three kinds of drop collisions: × for the binary collisions and ◆ for the ternary ones. The empty symbols correspond to binary collisions with immiscible liquids: glycerol concentrations varying from 20 % to 60 % with silicon oil M3 (△) and silicon oil M10 (○), fixed concentration of glycerol (50 %) combined with various oils (□).

For typical low $Oh < 0.1$, ζ_{crit} is a constant equal to 3, a value close to π, as expected for the classical Rayleigh criterion. This result is actually surprising since this criterion is built without considering the cylinder extremities and for quasi-static situations. A closer look at the geometry of the relaxing cylinder suggests to assimilate its extremities to hemispheres. Doing so, and considering surface energy only, leads to a critical value of approximately 3.73, larger than the observed one. The deviation could originate from the fact that the cylinder is not under quasi-static conditions, but rather contains internal flows (Qian & Law 1997). This is in agreement with the numerical simulations where the internal kinetic energy is non-zero above the fragmentation threshold, see figure 7. This can also be evidenced on the photographs of collisions just above the threshold, showing the just separated drops with a relative movement, trace of the remaining stored kinetic energy.

Taking into account the kinetic energy corresponding to the internal flow requires the full determination of the flow field and the exact shape of the relaxing liquid system. A reasonable estimation may be obtained estimating the dynamic pressure by the difference of Laplace pressure between the central part of the cylinder and one hemispherical cap ($\rho v^2/2 \approx 2\sigma/d$ with d, the cylinder diameter). The velocity can thus be integrated on the cylindrical volume found between the two spherical caps ($\pi d^2(l-d)/4$ with l, the distance between the centre of the two spherical caps). Although accounting for the internal flow in this way is quite crude, it gives a critical value of 2.83, closer to the experimental result than the predicted quasi-static value.

The validity limit of this adapted Rayleigh criterion ($Oh < 0.1$) can be understood comparing the time scale of bulk motion, t_B, to the time scale of interfacial motion t_{oscill}. Interfacial curvature induces a stress via the Laplace pressure, driving a flow whose time scale is $t_B = \mu D/\sigma$ (Stone & Leal 1989). The time scale at which the interface contracts corresponds to a fraction of an oscillation period $t_{oscill} = \sqrt{\rho D^3/\sigma}$ (Rayleigh 1879) and $t_B/t_{oscill} = Oh$. For large Oh, the bulk flows faster than the interface contracts. As a result, the outward internal flow drains the central part of the transient cylinder in its two extremities, forming a dumbbell. The previous criterion built on a cylinder does not hold then.

https://doi.org/10.1017/jfm.2016.852 Published online by Cambridge University Press

3.3. *Relaxation*

The energy balance for the relaxation phase reads:

$$E_{\sigma,disk} = E_{K,cyl} + E_{\sigma,cyl} + E_{\mu,relax}, \tag{3.12}$$

where $E_{K,cyl}$ is the kinetic energy stored in the cylinder, $E_{\sigma,cyl}$ the surface energy of the cylinder and $E_{\mu,relax}$ the energy dissipated during the relaxation phase. The very moderate relative motion of the drops just above the fragmentation threshold (figure 2f), as well as the results of the numerical calculations (figure 7), suggest that $E_{K,cyl}$ is negligible in (3.12). Using the results of § 3.1, equation (3.12) becomes

$$(1-a)E_{K,ini} + E_{\sigma,ini} = E_{\sigma,cyl} + E_{\mu,relax}. \tag{3.13}$$

3.3.1. *Estimating $E_{\sigma,ini} - E_{\sigma,cyl}$ at the fragmentation threshold*

At the fragmentation threshold, two drops of equal sizes are produced (Rayleigh criterion). For binary collisions, the volume conservation requires that these two drops have the diameter D of the initial drops. Consequently, the surface energy of the drops resulting from the fragmentation, which is by definition equal to the one of the cylinder, $E_{\sigma,cyl}$, must be equal to $E_{\sigma,ini}$. We deduce $E_{\sigma,cyl} = E_{\sigma,ini}$.

In the case of ternary collisions, we obtain: $E_{\sigma,ini} - E_{\sigma,cyl} = (1-(2/3)^{1/3})E_{\sigma,ini}$ which can also be expressed as $72(1-(2/3)^{1/3})E_{K,ini}/We$.

For collisions with immiscible liquids, this energy difference depends on the distribution of the encapsulated liquid within the two resulting drops. It can be written as: $E_{\sigma,ini} - E_{\sigma,cyl} = \pi D^2(\sigma_w - \sigma_o - 2\omega\sigma_{ow})$ where ω varies from $2^{-2/3} \approx 0.63$ for equally distributed liquids to 0.5 in the limit case where all the encapsulated liquid is in one drop only. The relative variations are quite small, and for a given combination of surface and interfacial tensions $E_{\sigma,ini} - E_{\sigma,cyl}$ can be regarded as constant.

3.3.2. *Scaling relations for $E_{\mu,relax}$*

The estimation of the viscous losses during the relaxation phase is quite difficult. There exist different sources of velocity gradients, such as the Laplace pressure difference between the torus and the lamella responsible for the torus to drain into the lamella, as well as the interface retraction for the minimization of surface energy and resulting in the collapse of the torus. The length scales are also very different, involving large dimensions (D, D_{max} and L_{max}, the maximal cylinder length) and much smaller ones, such as the thickness of the lamella h or of the viscous boundary layer l_μ. To approach this problem, we distinguish different sub-periods or sub-cases during the relaxation, as in the work of Qian & Law (1997) and Roisman (2004). Schematically, the first one extends until the lamella disappears engulfed in the retracting torus, the second one follows until the cylinder reaches its maximal elongation and eventually breaks up. This evolution is represented in figure 13.

(i) First instants.

For the first sub-period, the general expression of the viscous losses reads

$$E_{\mu,relax,3} = \mu\left(\frac{\Delta V}{\Delta X}\right)^2 \Omega_3 T_3. \tag{3.14}$$

This sub-period corresponds more or less to the relaxation of a distorted drop in the oblate phase. The time period T_3 scales as t_{oscill} and the velocity ΔV as $D_{max}/t_{oscill} \approx U$. We thus expect, as for the compression phase, the velocity variations to remain limited to the viscous boundary layer of thickness $l_\mu = \mu/\rho U$. We obtain the velocity gradient

https://doi.org/10.1017/jfm.2016.852 Published online by Cambridge University Press

$\Delta V/\Delta X \approx \rho U^2/\mu$. The volume Ω_3 is difficult to estimate. We propose to estimate this volume as the overlap of the lamella and the torus. As a result, Ω_3 scales like the lamella thickness (again estimated by $\sigma/\rho U^2$) and a part of the torus immediately at the contact with the lamella, estimated by r_{rim}^2. This leads to $\Omega_3 \approx (D^2\sigma)/(\rho We^{1/2}U^2)$. The losses scale as

$$E_{\mu,relax,3} \approx b\frac{\rho U^2 D^3}{OhWe^{1/2}}, \tag{3.15}$$

where b is a constant. This expression is valid as long as $b/(OhWe^{1/2})$ is less than $(1-a)$.

(ii) Cylinder elongation.

During the second sub-period, which can be seen as a drop oscillation in the prolate phase, the losses read

$$E_{\mu,relax,4} = \mu\left(\frac{\Delta V}{\Delta X}\right)^2 \Omega_4 T_4. \tag{3.16}$$

To estimate the velocity gradient, the velocity V is approximated by L_{max}/T_4, with L_{max} the maximal length reached by the cylinder, and T_4 the oscillation time scale of the merged drop. By analogy with a water spring, the liquid complex relaxes over a time scale of $\sqrt{2}t_{oscill}$ and $\sqrt{3}t_{oscill}$ for the binary and ternary cases, respectively. Similarly, the variations of velocity typically take place on $2^{1/3}D$ and $3^{1/3}D$. Finally, the volume Ω_4 can be estimated by $2D^3$ and $3D^3$ for binary and ternary cases. Following these scalings leads to

$$E_{\mu,relax,4} = \mu\left(\frac{L_{max}}{2^{1/3}D}\right)^2 \frac{\sqrt{2}D^3}{t_{oscill}} \quad \text{binary collisions,} \tag{3.17}$$

$$E_{\mu,relax,4} = \mu\left(\frac{L_{max}}{3^{1/3}D}\right)^2 \frac{\sqrt{3}D^3}{t_{oscill}} \quad \text{ternary collisions.} \tag{3.18}$$

(iii) On the relative importance of these losses.

The distinction between the two sub-periods is rather arbitrary, since the disk retraction and the cylinder elongation do not happen sequentially, but rather in parallel. The liquid system at the end of the compression is neither a pancake nor an ellipsoid, which makes the first instants of its retraction difficult to describe. Qualitatively, its phenomenology depends on its exact shape, and the two extreme cases represented in figure 14 can be distinguished. Denoting D_{merged} as the diameter of the merged drop ($D_{merged} = 2^{1/3}D$ or $3^{1/3}D$), the first limit corresponds to large D_{max}/D_{merged}. For a given We, D_{max}/D_{merged} is larger for binary than for ternary collisions, and it increases with We for a given collision type. In the limit where D_{max}/D_{merged} is comparable to unity, the flux from the torus to the lamella remains small since the Laplace pressure gradient is moderate. The torus collapses on itself. The velocity gradients are mainly limited to the viscous boundary layer, and the losses occur on the volume corresponding to the overlap of the lamella with the torus. The scaling proposed for $E_{\mu,relax,3}$ seems relevant. After this collapse, the cylinder extends and further losses are expected in the form of $E_{\mu,relax,4}$. The total losses can be estimated by summing up $E_{\mu,relax,3}$ and $E_{\mu,relax,4}$. For large D_{max}/D_{merged}, the small rim radius ($r_{rim} \propto DWe^{-1/4}$) induces a large pressure gradient which drains the torus into the

https://doi.org/10.1017/jfm.2016.852 Published online by Cambridge University Press

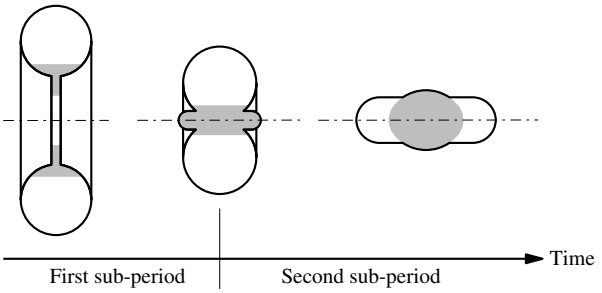


FIGURE 13. Schematic temporal evolution of the disk relaxing into a cylinder (cross-section). During the first sub-period, the lamella is engulfed in the collapsing torus. In the second one, the cylinder elongates. The volumes assumed to have the highest velocity gradients are shown in grey.

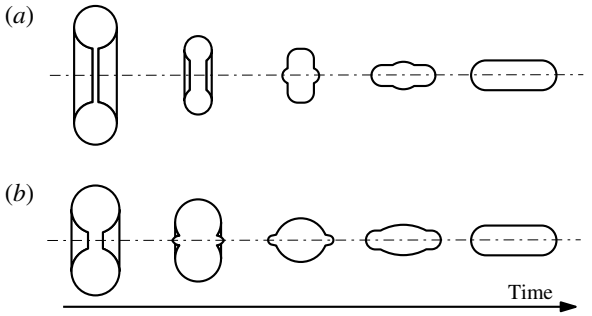


FIGURE 14. Possible evolution (qualitative) of the liquid complex during relaxation (cross-section). (*a*) Laplace pressure gradients drain the torus in the lamella before it collapses. (*b*) The torus collapses on itself, engulfing the lamella.

lamella before the disk significantly retracts (retraction velocity scales as D_{max}/t_{oscill}). The scaling proposed for the losses of the first instants, based on the torus collapse, is not fully relevant any more, and the total losses are expected to scale as $E_{\mu,relax,4}$, the expression proposed for the second sub-period.

For drop collisions with immiscible liquids, this approach must be modified to take into account the structure of the merged entity which consists of an aqueous core and an encapsulating oil shell. As already reported in Planchette *et al.* (2012), the losses are assumed to be mainly located in the oil shell, which provides the scaling

$$E_{\mu,relax} \approx \mu_o \frac{L_{max}}{D} \frac{D^3}{t_{oscill,o}}. \tag{3.19}$$

Here $t_{oscill,o}$ is calculated using the density and surface tension of the oil.

3.4. *Threshold velocity* U_t

3.4.1. *Scaling laws*

With the help of the modified Rayleigh criterion (see figure 12), L_{max}/D can be taken equal to $\zeta_{crit} d/D$ where d is the cylinder diameter, for all collisions with $Oh < 0.1$.

https://doi.org/10.1017/jfm.2016.852 Published online by Cambridge University Press

For binary collisions with one liquid, combining the results of § 3.1, the facts that $E_{\sigma,ini} = E_{\sigma,cyl}$ and $d/D \approx 0.8$, with the scaling obtained for $E_{\mu,relax}$ (3.15) and (3.17), provides the theoretical threshold velocity

$$U_{t,2D}^{theo} = 0.8\zeta_{crit}\sqrt{\frac{24\sqrt{2}/\pi}{1 - a - b_{2D}/(We^{1/2}Oh)}}\sqrt{\frac{\mu}{\rho\, t_{oscill}}}. \tag{3.20}$$

For ternary collisions, $d/D \approx 0.9$ and we similarly obtain

$$U_{t,3D}^{theo} = 0.9\zeta_{crit}\sqrt{\frac{24\sqrt{3}/\pi}{1 - a - b_{3D}/(We^{1/2}Oh) + 72/(We(1-(2/3)^{1/3}))}}\sqrt{\frac{\mu}{\rho\, t_{oscill}}}, \tag{3.21}$$

where b_{2D} and b_{3D} are two constants specifying the relative importance of the losses in the first and second sub-periods of the relaxation.

For binary collisions with immiscible liquids, the scaling law accounting for surface energy variations, is

$$U_{t,IM}^{theo} \approx \sqrt{A\zeta_{crit}\frac{\mu_o}{\rho_o + \rho_w}\sqrt{\frac{\sigma_o}{\rho_o D^3}} - \frac{48(\sigma_w - \sigma_o - 2w\sigma_{ow})}{(1 - a_I)(\rho_o + \rho_w)D}}, \tag{3.22}$$

where A is a constant. By treating the surface energy terms as a constant, as in Planchette *et al.* (2012), it simplifies to:

$$U_{t,IM}^{theo} \approx 50\sqrt{\zeta_{crit}\frac{\mu_o}{\rho_o + \rho_w}\sqrt{\frac{\sigma_o}{\rho_o D^3}}}. \tag{3.23}$$

This modelling approach is *a priori* valid as long as the Rayleigh criterion is followed, i.e. for $Oh < 0.1$.

3.4.2. *Comparison to experimental results*

For each kind of collision we experimentally determined the fragmentation threshold using a wide range of liquid properties ($887 < \rho < 1935$ kg m^{-3}, $1.2 < \mu < 19.3$ mPa s and $17.8 < \sigma < 68.9$ mN m^{-1}) and droplet diameters (between 130 and 870 μm). Practically, the threshold velocity is taken as the average of the highest velocity leading to coalescence and the lowest one resulting in fragmentation, which corresponds to typical errors of ± 0.05 m s^{-1}. These experimental thresholds are plotted in figure 15 as a function of the theoretical ones $U_{t,2D}^{theo}$, $U_{t,3D}^{theo}$. The scaling predictions are first evaluated with b_{2D} and b_{3D} equal to zero, a equals to $a_{plat,2D}$ and $a_{plat,3D}$ for values of $\alpha(We^{1/4} + \beta We^{-1/4})/Re$ corresponding to the plateaus and with the values of a estimated in figure 10 for other cases. For collisions with immiscible liquids, the value $a_I = 0.97$ is integrated in the prefactor of (3.23), and $\zeta_{crit} = 3$ for all cases. Overall, the agreement between the predictions and the experimental data is very good. Given the variety of configurations considered, it indicates that our modelling approach is very general and meaningful. The results obtained with immiscible liquids (not reproduced here) are very satisfactory, as already reported in Planchette *et al.* (2012). For the binary collisions with one liquid, we observe good agreement for the points corresponding to $Oh < 0.1$. These points are found along a line through the origin with a slope of 2.5, indicating the right order of magnitude.

https://doi.org/10.1017/jfm.2016.852 Published online by Cambridge University Press

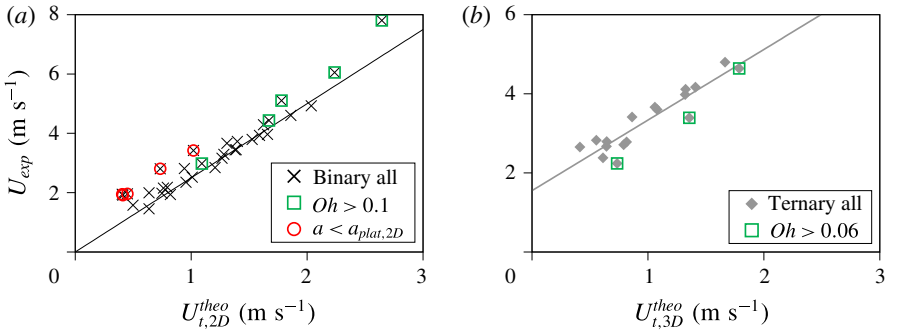


FIGURE 15. (Colour online) Experimental threshold velocity U_{exp} as a function of the theoretical predictions U_t^{theo}. (*a*) Binary collisions $U^{theo}_{t,2D}$ is evaluated with (3.20) taking $b_{2D} = 0$. The diagonal line indicates a slope of 2.5. (*b*) Ternary collisions $U^{theo}_{t,3D}$ is evaluated with (3.21) taking $b_{3D} = 0$.

The validity limit of the Rayleigh criterion explains the validity limit of the predictions for higher Oh. It is interesting to note that by excluding the data points for $Oh > 0.1$, we also exclude the points corresponding to $\alpha(We^{1/4} + \beta We^{-1/4})/Re > 0.01$ found in the third regime of figure 10. The velocity threshold predicted for the points found in the first regime of figure 10 for which $a < a_{plat,2D}$ are underestimated.

The agreement is also very good for ternary collisions. The slope between the experimental and theoretical points is similar to the one observed for binary collisions (1.8 instead of 2.5). In contrast to the binary collisions we note the existence of a relatively large intercept corresponding to an underestimation of the threshold and tending to decrease with increasing Oh. We do not explain this intercept by the difference between $E_{\sigma,ini}$ and $E_{\sigma,cyl}$, since we accounted for it in our scaling.

Including the losses of the first relaxation sub-period allows to reduce the deviations for binary collisions at low values of a as well as the intercept for the ternary collisions. The results are presented in figure 16 where the scaling laws are evaluated with $b_{2D} = 0.025(1 - a_{2D})$ and $b_{3D} = 0.08(1 - a_{3D})$. The reason for taking b_{2D} and b_{3D} as functions of $(1 - a_{2D})$ and $(1 - a_{3D})$, respectively, comes from the dependency of the excess surface energy on $(1 - a)$. Indeed, the excess surface energy available at the end of the compression scales as $E_{\sigma,disk} - E_{\sigma,ini} \approx E_{K,ini}(1 - a)$. Thus, the losses caused by the collapse of the torus on itself may increase with increasing $(1 - a)$. With this correction, the agreement becomes excellent for the binary collisions. Indeed, all experimental points satisfying the Rayleigh criterion ($Oh < 0.1$) are represented in figure 16. This includes glycerol solutions with concentrations ranging from 10 % to 65 %, silicon oils and drop diameters between 130 and 870 μm. All these points are found well aligned, so that the experimental threshold, U_{exp}, is well predicted by $2.38\,U^{theo}_{t,2D}$. For ternary collisions, the intercept is reduced from 1.55 to 0.61, which indicates the relevance of this correction. Note that for one point corresponding to $Oh = 0.06$ the correction could not be applied because $b/(OhWe^{1/2}) > 1 - a$. All other experimental data points obtained for ternary collisions are shown in figure 16. The liquids include glycerol solutions with concentrations varying between 30 % and 70 % and silicon oils, while the drop diameters range between 130 and 550 μm. For all these cases, U_{exp} can be very well approached by $2.20\,U^{theo}_{t,3D} + 0.61$. Besides the difficulties to estimate the losses in the relaxation phase, it seems that our analysis is

https://doi.org/10.1017/jfm.2016.852 Published online by Cambridge University Press

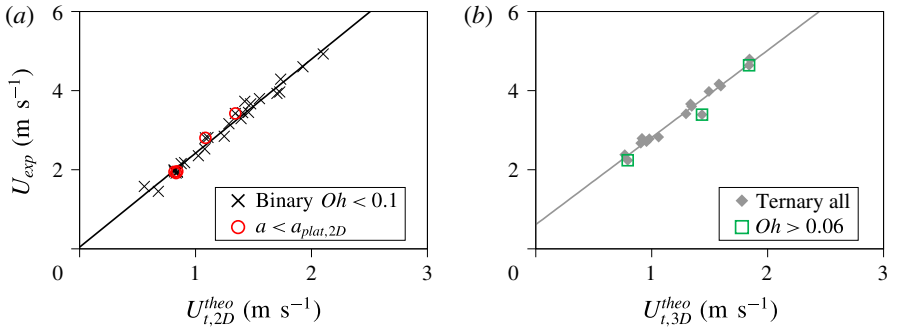


FIGURE 16. (Colour online) Experimental threshold velocity U_{exp} versus the theoretical prediction U_t^{theo}. (*a*) Binary collisions $U_{t,2D}^{theo}$ evaluated with (3.20), taking $b_{2D} = 0.025(1 - a_{2D})$. (*b*) Ternary collisions $U_{t,3D}^{theo}$ evaluated with (3.21), taking $b_{3D} = 0.08(1 - a_{3D})$.

qualitatively correct and that, even though the sum of proposed scalings is tentative, the result captures the major contributions properly.

Finally, it is interesting to reformulate, for collisions using one liquid, the threshold velocity in terms of a critical *Re* versus a critical *Oh*, as represented in Planchette *et al.* (2012) and Hinterbichler *et al.* (2015). The exponents deduced from fitting the critical experimental *Re* as a power of *Oh* for $Oh < 0.1$ are -0.75 and -0.90 for binary and ternary collisions, respectively, using a subset of the data set of this paper. The change of exponent between the ternary and binary cases seems to indicate a principal difference between these configurations. Denoting a constant as *C*, the relations (3.20) and (3.21) assume the form

$$Re^2 \propto \frac{b}{1-a} Re\, Oh^{-2} + \frac{C}{1-a} Oh^{-1}. \tag{3.24}$$

Assuming *a* and *b* to be independent of *Oh* and *Re*, which is verified on a wide range of $\alpha(We^{1/4} + \beta We^{-1/4})/Re > 0.01$, we can derive three exponents corresponding to three limiting cases. If b/Oh^2 is negligible against the other terms, we obtain $Re \propto Oh^{-1/2}$. This is the case if most of the losses during relaxation occur during the second sub-period, in the entire liquid system. If *C* is small, e.g. when most of the relaxation losses are caused by the collapse of the torus on itself at the very first instants, *Re* scales as Oh^{-2}. Finally if *Re* is small enough to neglect the left-hand side of equation (3.24), i.e. for very large losses during the compression phase, the scaling reads $Re \propto Oh$. These exponents are different from those obtained by fitting the experimental data. Yet, the three terms are probably of the same order, and it may be difficult to further reduce (3.24). Indeed, re-plotting the experimental critical values of *Re* versus *Oh* in terms of critical *Re* versus *We* gives quite dispersed data points (plot not shown). Although the representation given in Hinterbichler *et al.* (2015) appears at first promising, it may be misleading due to the fact that $Oh = \sqrt{We}/Re$, which considerably reduces the dispersion with *We* in contrary to the proposed scalings.

4. Summary and conclusions

The onset of fragmentation in head-on drop collisions was experimentally investigated for binary collisions with one single liquid and two immiscible ones,

https://doi.org/10.1017/jfm.2016.852 Published online by Cambridge University Press

as well as for ternary collisions. The velocity thresholds were obtained for a wide range of drop diameters (from 130 to 870 μm), using a wide variety of liquids with surface tension and viscosity varying between 18 and 70 mN m^{-1} and between 1 and 20 mPa s, respectively. A general model predicting the velocity threshold of fragmentation for all three kinds of collisions was established. The model is based on two essential elements: the analogy between drops and liquid springs, and the use of the Rayleigh criterion at the fragmentation threshold. More precisely, colliding drops are seen as liquid springs that compress, merge and relax into a cylinder. For each sub-phase of the collision, energy balances are made, providing scaling laws which compare very well to experimental results. Especially the losses of the compression phase are found to be an increasing function of $\alpha(We^{1/4} + \beta We^{-1/4})/Re$, presenting a plateau for a wide range of $\alpha(We^{1/4} + \beta We^{-1/4})/Re$, which is in agreement with previous findings (Jiang *et al.* 1992; Willis & Orme 2003). The further use of the Rayleigh criterion led to the prediction of the threshold for $Oh < 0.1$. Given the variety of considered configurations, the wide range of droplet diameters and liquid properties at stake, our results indicate that this modelling approach, considering drops as liquid springs that merge, compress and relax into a cylinder which breaks up if its aspect ratio exceeds a critical value, captures very well the main physical contributions. The robustness of the model may motivate its extension to other, yet similar problems involving drops in the capillary–inertial regime.

Acknowledgements

M.L. and D.B. gratefully acknowledge financial support provided by the German Research Foundation (DFG) within the scope of SFB-TRR 75. Support for H.H. from the Research Center Pharmaceutical Engineering GmbH at Graz University of Technology is gratefully acknowledged. We acknowledge support from the COST action MP1106.

REFERENCES

ASHGRIZ, N. & POO, J. Y. 1990 Coalescence and separation in binary collisions of liquid drops. *J. Fluid Mech.* **221**, 183–204.

BAZILEVSKII, A. V., VORONKOV, S. I., ENTOV, V. M. & ROZHKOV, A. N. 1981 Orientational effects in the decomposition of streams and strands of diluted polymer solutions. *Sov. Phys. Dokl.* **26**, 333–335.

BIANCE, A.-L., CHEVY, F., CLANET, C., LAGUBEAU, G. & QUÉRÉ, D. 2006 On the elasticity of an inertial liquid shock. *J. Fluid Mech.* **554**, 47–66.

BRAZIER-SMITH, P. R., JENNINGS, S. G. & LATHAM, J. 1972 The interaction of falling water drops: coalescence. *Proc. R. Soc. Lond.* **326**, 393–408.

CHEN, R.-H. & CHEN, C.-T. 2006 Collisions between immiscible drops with large surface tension difference: diesel oil and water. *Exp. Fluids* **41**, 453–461.

DAI, M. & SCHMIDT, D. P. 2005 Numerical simulation of head-on droplet collision: effect of viscosity on maximum deformation. *Phys. Fluids* **17**, 041701.

FOCKE, C. & BOTHE, D. 2011 Computational analysis of binary collisions of shear-thinning droplets. *J. Non-Newtonian Fluid Mech.* **166**, 799–810.

FOCKE, C. & BOTHE, D. 2012 Direct numerical simulation of binary off-center collisions of shear thinning droplets at high Weber numbers. *Phys. Fluids* **24**, 073105.

FOCKE, C., KUSCHEL, M., SOMMERFELD, M. & BOTHE, D. 2013 Collision between high and low viscosity droplets: direct numerical simulations and experiments. *Intl J. Multiphase Flow* **56**, 81–92.

https://doi.org/10.1017/jfm.2016.852 Published online by Cambridge University Press

GOTAAS, C., HAVELKA, P., JAKOBSEN, H. A., SVENDSEN, H. F., HASE, M., ROTH, N. & WEIGAND, B. 2007 Effect of viscosity on droplet–droplet collision outcome: experimental study and numerical comparison. *Phys. Fluids* **19** (10), 102106.

HINTERBICHLER, H., PLANCHETTE, C. & BRENN, G. 2015 Ternary drop collisions. *Exp. Fluids* **56**, 190.

HIRT, C. W. & NICHOLS, B. D. 1981 Volume of fluid (VOF) method for the dynamics of free boundaries. *J. Comput. Phys.* **39**, 201–225.

JIANG, Y. J., UMEMURA, A. & LAW, C. K. 1992 An experimental investigation in the collision behaviour of hydrocarbon droplets. *J. Fluid Mech.* **234**, 171–190.

LAFAURIE, B., NARDONE, C., SCARDOVELLI, R., ZALESKI, S. & ZANETTI, G. 1994 Modelling merging and fragmentation in multiphase flows with surfer. *J. Comput. Phys.* **113**, 134–147.

LIU, M. & BOTHE, D. 2016 Numerical study of head-on droplet collisions at high Weber numbers. *J. Fluid Mech.* **789**, 785–805.

LYCETT-BROWN, D., LUO, K. H., LIU, R. & LV, P. 2014 Binary droplet collision simulations by a multiphase cascaded lattice Boltzmann method. *Phys. Fluids* **26** (2), 023303.

MONTGOMERY, D. N. 1970 Collision and coalescence of water drops. *J. Atmos. Sci.* **28**, 291–293.

NIKOLOPOULOS, N., NIKAS, K.-S. & BERGELES, G. 2009 A numerical investigation of central binary collision of droplets. *Comput. Fluids* **38**, 1191–1202.

NOBARI, M. R., JAN, Y.-J. & TRYGGVASON, G. 1996 Head-on collision of drops – a numerical investigation. *Phys. Fluids* **8**, 29–42.

OKUMURA, K., CHEVY, F., RICHARD, D., QUÉRÉ, D. & CLANET, C. 2003 Water spring: a model for bouncing drops. *Europhys. Lett.* **62** (2), 237–243.

PLANCHETTE, C., LORENCEAU, E. & BRENN, G. 2012 The onset of fragmentation in binary liquid drop collisions. *J. Fluid Mech.* **702**, 5–25.

QIAN, J. & LAW, C. K. 1997 Regimes of coalescence and separation in droplet collision. *J. Fluid Mech.* **331**, 59–80.

RAYLEIGH, LORD 1879 On the capillary phenomena of jets. *Proc. R. Soc. Lond.* **29**, 71–97.

RICHARD, D., CLANET, C. & QUÉRÉ, D. 2002 Surface phenomena: contact time of a bouncing drop. *Nature* **417** (6891), 811.

ROISMAN, I. V. 2004 Dynamics of inertia-dominated binary drop collisions. *Phys. Fluids* **16** (9), 3438–3449.

ROISMAN, I. V. 2009*a* Inertia dominated drop collisions. i. On the universal flow in the lamella. *Phys. Fluids* **21** (5), 052103.

ROISMAN, I. V. 2009*b* Inertia-dominated drop collisions. ii. An analytical solution of the Navier–Stokes equations for spreading viscous film. *Phys. Fluids* **21** (5), 052104.

ROISMAN, I. V., PLANCHETTE, C., LORENCEAU, E. & BRENN, G. 2011 Binary collisions of drops of immiscible liquids. *J. Fluid Mech.* **690**, 512–535.

SAROKA, M. D., ASHGRIZ, N. & MOVASSAT, M. 2012 Numerical investigation of head-on binary drop collisions in a dynamically inert environment. *J. Appl. Fluid Mech.* **5** (1), 23–37.

STONE, H. A. & LEAL, L. G. 1989 Relaxation and breakup of an initially extended drop in an otherwise quiescent fluid. *J. Fluid Mech.* **198**, 399–427.

SYMON, K. R. 1971 *Mechanics*, 3rd edn. Addison-Wesley.

TAYLOR, G. I. 1959 The dynamics of thin sheets of fluid ii. Waves on fluid sheets. *Proc. R. Soc. Lond.* A **263**, 296–312.

WILLIS, K. D. & ORME, M. 2000 Experiments on the dynamics of droplet collisions in a vacuum. *Exp. Fluids* **29**, 347–358.

WILLIS, K. D. & ORME, M. 2003 Binary droplet collisions in a vacuum environment: an experimental investigation on the role of viscosity. *Exp. Fluids* **34**, 28–41.

YEO, Y., CHEN, A. U., BASARAN, O. A. & PARK, K. 2004 Solvent exchange method: a novel microencapsulation technique using dual microdispensers. *Pharmaceut. Res.* **21**, 1419–1427.

https://doi.org/10.1017/jfm.2016.852 Published online by Cambridge University Press